POLITECNICO DI TORINO
Repository ISTITUZIONALE

Development and validation of a 1D-CFD combustion and emission model for a diesel hydrogen dual fuel marine medium-speed engine

Original
Development and validation of a 1D-CFD combustion and emission model for a diesel hydrogen dual fuel marine medium-speed engine / Stanzione, G., Piano, A., Millo, F., Vichi, G., Fiorini, N.. - In: INTERNATIONAL JOURNAL OF HYDROGEN ENERGY. - ISSN 0360-3199. - 252:(2026). [10.1016/j.ijhydene.2026.156136]

Availability:
This version is available at: 11583/3012851 since: 2026-07-08T15:20:05Z

Publisher:
Elsevier Ltd

Published
DOI:10.1016/j.ijhydene.2026.156136

Terms of use:

This article is made available under terms and conditions as specified in the corresponding bibliographic description in the repository

Publisher copyright

(Article begins on next page)

22 November 2026

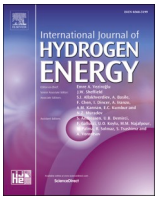
International Journal of Hydrogen Energy 252 (2026) 156136



Contents lists available at ScienceDirect

International Journal of Hydrogen Energy

journal homepage: www.elsevier.com/locate/he





Development and validation of a 1D-CFD combustion and emission model for a diesel hydrogen dual fuel marine medium-speed engine

Gerardo Stanzione [a], Andrea Piano [a,*], Federico Millo [a], Giovanni Vichi [b], Niccolò Fiorini [b]

[a] Politecnico di Torino, C.so Duca degli Abruzzi, 24, Torino, Italy
[b] YANMAR R&D Europe Srl, Viale Galileo, 3/A, Firenze, Italy

A B S T R A C T

Hydrogen utilization in internal combustion engines represents a promising pathway due to its negligible carbon content. Within this framework, this work presents novel combustion and emissions models for a diesel–hydrogen dual-fuel engine, enabling efficient system-level analysis. A compression-ignition engine retrofitted from conventional diesel operation was selected as a test case and modified with a port fuel injection system to supply gaseous hydrogen. The combustion model is based on an ignition delay metamodel derived from detailed chemical kinetics, capturing both the promoting and inhibiting effects of hydrogen on diesel ignition. Additionally, the spray penetration model was modified, improving agreement with experimental data across all investigated conditions. The model was validated against an extensive experimental campaign, achieving low RMSE values for MFB50 and burn duration (1.20 deg and 1.61 deg, respectively). Finally, a NOx emissions sub-model was integrated, confirming the accuracy and robustness of the proposed simulation framework.

1. Introduction

The transportation sector is a significant contributor to global greenhouse gas emissions. Growing concerns about climate change have driven the search for innovative solutions to reduce the environmental impact of engines [1]. In addition, the International Maritime Organization (IMO) implemented Tier III standards, which impose substantial restrictions on nitrogen oxides (NOx) emissions in designated Emission Control Areas (ECA). The objective of these new standards, which markedly curtail emissions in comparison to the Tier II limit, is to mitigate air pollution from maritime transport, thereby enhancing air quality in coastal regions and reducing the environmental impact of shipping activities [2,3]. Among the numerous emerging technologies, hydrogen has emerged as a promising alternative fuel, offering a viable solution to reconcile sustainability with efficiency and performance [4]. H_2-Diesel Dual-fuel technology can facilitate a smoother transition to more sustainable fuel options without requiring substantial modifications to existing engine fueling systems. Hydrogen integration into the combustion cycle of a diesel engine presents several advantages. Primarily, hydrogen combustion produces water vapor as the main exhaust product, leading to a significant reduction in particulate matter compared with conventional diesel engines. However, the effect on nitrogen oxides (NOx) emissions depends on the hydrogen content and operating conditions. In some cases, the presence of water vapor can lower combustion temperatures, reducing NOx formation, whereas in other cases the higher adiabatic flame temperature of hydrogen can increase local temperatures, thereby promoting NOx formation. This feature makes hydrogen-diesel dual-fuel engines a promising solution for meeting increasingly stringent emissions regulations [5–7]. Moreover, incorporating hydrogen into diesel fuel can enhance the engine's thermal efficiency. Hydrogen's ability to accelerate combustion leads to improved engine performance and reduced specific fuel consumption [8]. Despite the many advantages, the large-scale introduction of hydrogen-diesel engines presents some challenges. These include the high cost of hydrogen production and distribution, the need to develop safe and efficient storage systems, and the need to adapt refueling infrastructure. However, for maximum environmental benefit, it is essential to use hydrogen derived from renewable sources, such as solar or wind-powered water electrolysis. This approach aligns with the broader goal of minimizing the carbon footprint of transportation systems [9]. Karimi et al. [10] presented an in-depth review of the current knowledge about the dual-fuel internal combustion engine, focusing on its performance and emissions. Specific aspects under discussion include engine configuration, experimental results, and the available technologies or strategies to improve performance and emissions of this type of engine. However, continued research and development efforts are necessary to address technical challenges, including the hydrogen refueling system and storage, and ensure widespread implementation. If successfully optimized, hydrogen-diesel dual-fuel engines could play a pivotal role in the transition to a cleaner and more sustainable

* Corresponding author.
E-mail address: andrea.piano@polito.it (A. Piano).

https://doi.org/10.1016/j.ijhydene.2026.156136
Received 9 February 2026; Received in revised form 15 May 2026; Accepted 16 June 2026
Available online 25 June 2026
0360-3199/© 2026 The Authors. Published by Elsevier Ltd on behalf of Hydrogen Energy Publications LLC. This is an open access article under the CC BY license (http://creativecommons.org/licenses/by/4.0/).

transportation system [10]. In their study, Liu et al. [11] examined the combustion and emissions behavior of a hydrogen-diesel dual-fuel internal combustion engine under several engine loads. They investigated the impact of exhaust gas recirculation (EGR), diesel pilot injection timing, and hydrogen substitution rate on the engine's performance. Their analysis revealed that, in dual-fuel mode, the equivalent brake-specific fuel consumption ($BSFC_{eq}$) decreased as the engine load increased. Furthermore, a 4.6% improvement in thermal efficiency was observed under high engine load conditions. In addition, experimental findings indicated that, as expected, increasing the EGR can lead to a reduction in nitrogen oxides (NOx) emissions by up to 63%. Consequently, the impact of the timing of diesel pilot injection was assessed. It was demonstrated that delaying the injection process led to a decrease in NOx emissions due to a reduction of the in-cylinder temperature. However, this delay resulted in an 8.5% increase in carbon dioxide (CO_2) emissions. In a series of studies, researchers examined the impact of incorporating hydrogen into a compression-ignition engine fueled with cottonseed biodiesel [12,13]. In particular, Gurusamy et al. [12] investigated the effect of different hydrogen flow rates under several engine loads, highlighting that the ignition delay decreased, and the brake thermal efficiency increased as the hydrogen energy share increased under all engine loads. Moreover, the nitrogen oxides emissions increased with the increase of the hydrogen flow rate due to the increase of the in-cylinder temperature during combustion. Conversely, the emissions of other pollutants, including carbon monoxide (CO), hydrocarbons (HC), and soot, have been reduced due to the decrease in the amount of carbon present in the air-fuel mixture with an increase in the hydrogen fraction.

In light of these results, which demonstrated the potential for reducing emissions and enhancing efficiency through the utilization of hydrogen enrichment in a compression-ignition engine, the development of predictive modeling tools can support the analysis and optimization of this engine configuration. The latter could incorporate a zero-/one-dimensional (0D/1D) predictive combustion model that replicates combustion behavior and accurately predicts performance and emissions. However, the phenomenological simulation of dual fuel combustion presents a significant challenge for a 0D/1D combustion model due to the necessity of simulating the combustion process of two distinct fuels and their interaction. Numerous research studies have been published that propose various approaches for the replication of this particular combustion.

Parsa et al. [14] proposed two different approaches to replicate the ignition delay of a hydrogen-diesel dual fuel engine. A detailed chemistry simulation was employed to investigate the effect of hydrogen on the diesel ignition delay. The outcomes of this simulation were subsequently employed to train an Artificial Neural Network (ANN) to replicate the ignition delay. Barro et al. [15] employed a multi-Wiebe function to predict the two combustion phases. Taritas et al. [16] developed a model that describes the diesel injection by using a packet approach. Furthermore, the presence of multiple flame kernels ignited by the distinct diesel sprays was modeled by employing a multi-flame model. Millo et al. [17] developed and calibrated a multizone combustion model to predict the combustion process of a methane-diesel engine. A properly calibrated ignition delay correlation was employed to replicate the inhibitory effect of the gaseous fuel on the diesel start of combustion. Additionally, the prediction of laminar flame speed was improved by optimizing the formulation introduced by Metghalchi et al. [18].

Following on from other studies in the literature, this research analyzes the conversion of a medium-speed compression ignition (CI) internal combustion engine into a dual-fuel (DF) hydrogen-diesel internal combustion engine. A comprehensive experimental analysis is conducted to assess the impact of various engine parameters, including Hydrogen Energy Share (HES), engine load, and diesel and hydrogen injection parameters, on the performance and emissions of the engine. In addition, a predictive hydrogen-diesel dual-fuel combustion model is presented. The standard model, which is already available in GT-SUITE, was modified with a dedicated ignition delay metamodel. This was trained employing the results of a 0D-CFD detailed chemistry calculation. The aim was to compute the effect of the hydrogen addition on the diesel autoignition. Furthermore, the spray evolution model was modified to account for the end-of-injection phenomena within the diesel spray as the injected diesel mass decreased. In order to enhance the predictive capabilities of this predictive tool, an NOx model based on the Extended Zeldovich mechanism was developed. This model enables the prediction of nitrogen oxides emissions as a function of different engine parameters. The comprehensive simulation tool was validated against experimental outcomes from a wide-ranging experimental campaign conducted by YANMAR on a Compressed-Ignited (CI) Single-Cylinder Engine (SCE).

2. Case study

The experimental campaign was carried out on a single-cylinder diesel engine, which was modified to run with diesel and hydrogen, whose characteristics are highlighted in Table 1. The diesel fuel was directly injected into the cylinder via a Denso G4.5S common rail injection system, while a gas injector was employed to inject hydrogen into the intake port.

Fig. 1 shows a schematic view of the engine test setup. The intake path includes an air compressor, followed by a surge tank to prevent the occurrence of pressure pulsations. The engine is not equipped with an exhaust gas recirculation (EGR) system.

The JIS n°2 diesel fuel and commercial hydrogen were employed in this study, and their characteristics are presented in Table 2.

During the test campaign, the engine speed was maintained at 1200 rpm, and the intake pressure was modified to represent two distinct engine loads, corresponding to 50% and 75% engine load. In the following, these conditions are referred to as medium load and high load, respectively. A single diesel injection was employed to trigger hydrogen combustion. The experimental campaign was designed to evaluate the effects of varying hydrogen injection parameters such as

Table 1
Engine characteristics.

Engine type	4-stroke SCE
Bore x Stroke	107 x 127 mm
Displacement	1141 cc
Compression Ratio (CR)	14.3
Diesel pilot injection system	Denso G4.5S Common rail injection system
Hydrogen injection system	Port Fuel Injection (PFI)

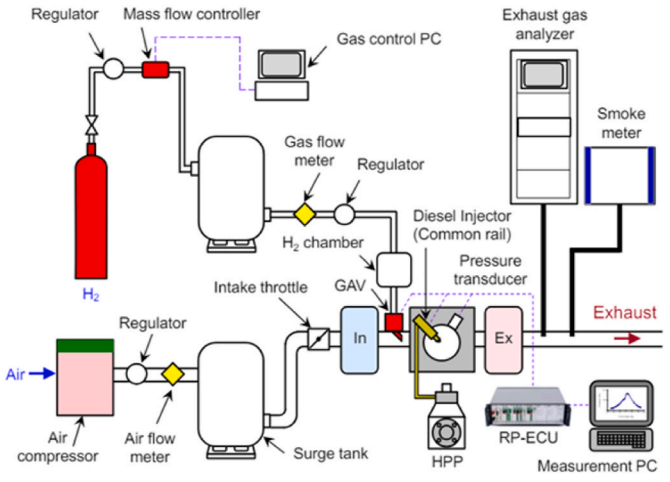


Fig. 1. – Test bench.

Table 2
Fuel properties.

Fuel	Density	H/C ratio	Lower heating value (LHV)	Stoichiometric mixing ratio
JIS n°2 diesel fuel	824.9 kg/m3	1.9	43.3 MJ/kg	14.7
Hydrogen	0.0899 kg/m3 (STP conditions)	-	120.0 MJ/kg	34.3

Table 3
Engine parameters sweep.

Engine speed	1200 rpm
Intake pressure	1.7 – 2.6 bar
Hydrogen injection pressure	4.2/5.7 bar
Hydrogen injection timing	-360/-260 deg aTDC
Diesel injection pressure	600/1200 bar
Diesel injection timing	-7/5 deg aTDC
Intake temperature	304/315 K

pressures and start of injection (SOI). Furthermore, the impact of modifying the diesel injection parameters, specifically the timing and pressure of the injection, was assessed. Moreover, the intake temperature was varied to investigate its effect on the engine performance. Table 3 provides a summary of the variations in experimental parameters.

Each sweep was extended considering different hydrogen/diesel shares. This was carried out by maintaining a constant total fuel energy input while modulating the injected hydrogen mass and pilot diesel quantity. The global excess air ratio (λ) was approximately 2 across all operating conditions. The Hydrogen Energy Share (HES), calculated as in Equation (1), has been used to monitor the different energy content.

$$HES = \frac{m_{H_2} \cdot LHV_{H_2}}{m_D \cdot LHV_D + m_{H_2} \cdot LHV_{H_2}} \quad \text{Eq. (1)}$$

Where, m_{H_2} is hydrogen injected mass [kg], LHV_{H_2} is hydrogen lower heating value [MJ/kg], m_D is diesel pilot fuel mass [kg], LHV_D is diesel lower heating value [MJ/kg].

3. Experimental analysis

3.1. Ignition delay analysis

The ignition delay is defined as the time required for the fuel to auto-ignite, and in this case, it was calculated as the difference between the hydraulic diesel start of injection (SOI_h) and the Start of Combustion (SOC). In this work, the SOC is defined as the crank angle corresponding to 0.1% of the burned mass fraction. This delay encompasses physical and chemical phenomena. The physical delay is due to the time required for the atomization, break-up, and evaporation of the liquid fuel. While, the chemical delay represents the interval between the initiation of the pre-combustion reactions and the onset of the auto-ignition. Both phenomena were influenced by the properties of the fuels as well as by the thermodynamic conditions of the mixture.

Fig. 2 depicts the ignition delay by reference to the hydrogen energy share under both medium and high load conditions. In both operating conditions, the diesel SOI has been kept unchanged during the sweep. It is evident that increasing the hydrogen substitution rate slightly increases the diesel ignition delay until it reaches approximately 60-70%. Then, a steep reduction of the ignition delay is visible, highlighting an increased mixture reactivity when hydrogen percentage increases. Moreover, under high engine load conditions, the ignition delay was shorter due to more favorable thermodynamic conditions in the combustion chamber. A similar trend was partially observed by Dhole et al. [19], who reported an initial increase in ignition delay with hydrogen

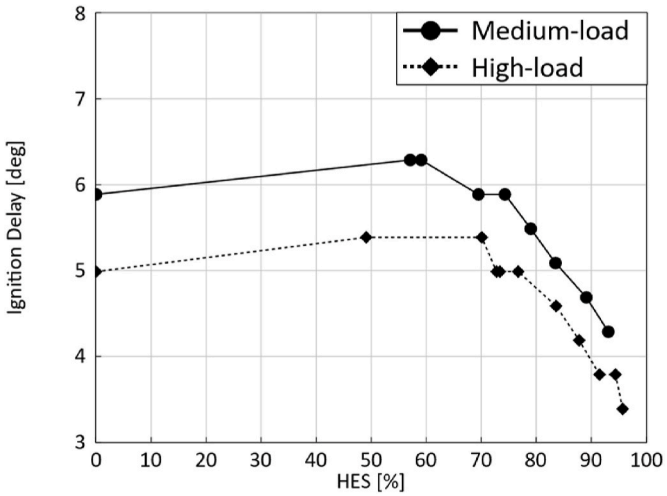


Fig. 2. Ignition Delay as a function of HES under medium and high engine load conditions.

substitution up to 20–30%, followed by a reduction at higher substitution levels. In contrast, Gurusamy et al. [12] observed a monotonic decrease in ignition delay with increasing hydrogen flow rate.

To better understand this behavior, the diesel injection rates and burn rates at medium-load are shown in Fig. 3.

In all cases, independently of the H2 percentage, a two-stage combustion process can be analyzed: firstly, the premixed diesel combustion causes a burn rate peak, whose intensity is linked to the amount of accumulated diesel fuel and the entrained hydrogen in the diesel spray. This phase is usually identified as spray combustion phase. Subsequently, 2 different combustion modes can exist depending on the HES: with high HES, the diesel spray ignition triggers the flame combustion, mainly driven by the turbulence level within the combustion chamber;

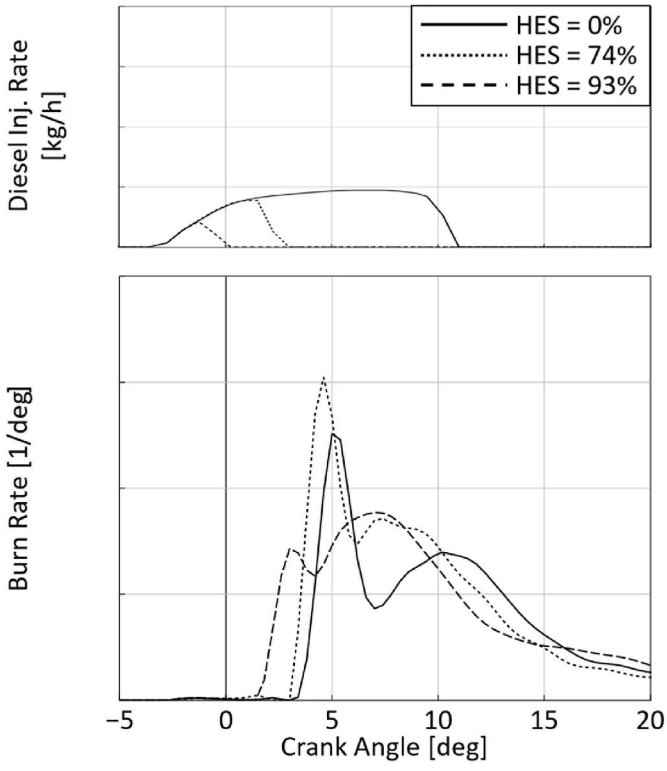


Fig. 3. Diesel injection rate (top) and measured burn rate (bottom) as a function of Crank Angle under medium engine load conditions.

while with low HES, the combustion is controlled by the diesel/air-hydrogen mixing rate. Moreover, keeping constant the diesel SOI and by increasing the hydrogen fraction, the reduction of the ignition delay is evident, as the reduction in the intensity of the first peak of the burn rate, accompanied by an increase of the flame combustion intensity due to the higher hydrogen content.

Gong et al. [20] calculated the effect of the hydrogen addition on the ignition delay of n-dodecane using a detailed chemistry simulation. They varied the hydrogen mass fraction from 0 to 0.9 and the temperature from 850 K to 1600 K, with constant pressure and equivalence ratio. The simulation outcomes highlighted that the hydrogen had an inhibitory effect when $T < 1050$ K, thus increasing the ignition delay with hydrogen mass fraction. When the $T > 1280$ K, an acceleration effect of hydrogen was observed, leading to a subsequent reduction in ignition delay as the hydrogen fraction increased. Conversely, when the temperature ranged from 1050 K to 1280 K, the ignition delay demonstrated a non-monotonic behavior with the increase of the hydrogen amount. Then, under the typical engine conditions, hydrogen may have an inhibitory effect on the autoignition of diesel fuel. Other explanations for the observed ignition delay behavior have been identified in the literature. Gurusamy et al. [12] attributed the reduction in ignition delay as the hydrogen amount increases to the higher hydrogen heating value and flame speed. These characteristics could lead to an increase in the temperature of the residual gas and, consequently, the temperature of the hydrogen-air mixture at the start of pilot injection. This increase could facilitate the evaporation of the liquid diesel fuel. Frerichs et al. [21] hypothesize that the overmixing caused by the entrainment wave after the conclusion of the injection process may facilitate the onset of combustion. Furthermore, the low-temperature heat release (LTHR) that occurs within the diesel spray could increase its temperature and facilitate the initiation of combustion. Musculus et al. [22,23] investigated the equivalence ratio in the diesel spray after the end of injection (EOI). Their results show that, for the same injected mass, the air-to-fuel (A/F) ratio increases by a factor of approximately three after 2 CAD compared to steady-jet conditions. This increase in the A/F ratio is primarily attributed to the entrainment waves generated at the end of injection, which enhance air entrainment into the diesel jet. This observation is consistent with the trend shown in Fig. 3, where advancing the end of injection (EOI) while keeping the start of injection (SOI) constant results in a reduction of the ignition delay.

3.2. Emissions analysis

Now, the focus moves to the analysis of the emissions. The impact of the hydrogen energy share is analyzed, as shown in Fig. 4. It shows the NOx and CO_2 emissions by reference to the percentage of hydrogen energy under medium and high load conditions.

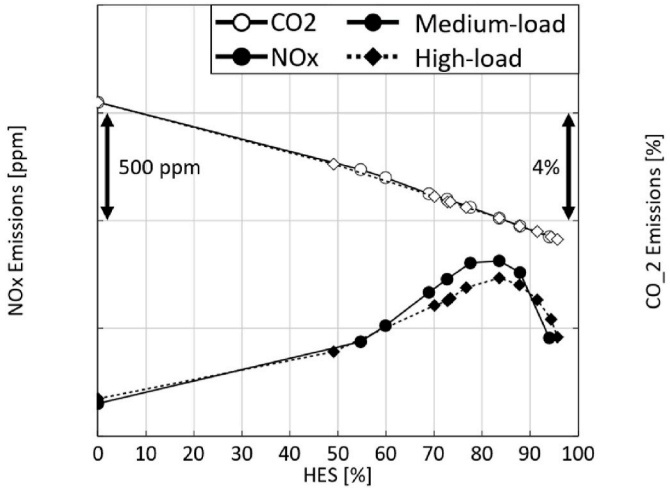


Fig. 4. NOx and CO_2 emissions vs HES at medium and high engine load.

First of all, the NOx emissions were assessed. It was observed that as the hydrogen amount increased up to approximately 85%, a corresponding rise in NOx emissions can be noticed for both the engine loads. As illustrated in Fig. 3, this phenomenon can be attributed to the increase in the first burn rate peak caused by hydrogen entrained within the diesel spray. This led to an increase in the in-cylinder pressure and temperature, which, consequently, resulted in elevated NOx emissions. The further increment of the hydrogen energy share (>85%) leads to a reduction of the NOx emissions, although the level observed in the diesel-only case is not reached. This phenomenon could be attributed to a decrease in the amount of diesel fuel, which led to a reduction in premixed combustion heat release, without a considerable increase in the burn rate during the hydrogen flame propagation phase (Fig. 3). Moreover, the reduction in the ignition delay caused a reduction in the time available for the diesel-hydrogen-air mixing, which led to a reduction in the hydrogen quantity that burns in the premixed combustion phase. The reduction of the premixed combustion heat release led to a decrease in the pressure rise rate, which resulted in a reduction of the maximum pressure and temperature in the combustion chamber.

Regarding CO_2 emissions, as shown in Fig. 4, increasing the hydrogen energy share led to a reduction in CO_2 emissions. This behavior is attributed to the substitution of diesel fuel with hydrogen, resulting in a lower carbon input to the combustion process. Consequently, the reduced diesel mass decreases the carbon content in the combustion chamber and, in turn, CO_2 emissions.

A similar trend was observed by Lata et al. [5], who reported an initial reduction in NOx emissions with hydrogen substitution up to 20%, followed by a slight increase at higher substitution levels under high-load conditions. Under low-load operation, hydrogen substitution led to a monotonic reduction in NOx emissions. In contrast, Gurusamy et al. [12] observed a monotonic increase in NOx emissions with increasing hydrogen flow rate, along with a decrease as engine load increased. Moreover, their results are consistent with the CO_2 emission trends shown in Fig. 4.

Variations in the other engine parameters resulted in NOx emission trends similar to those observed for diesel-only operation and are therefore not further discussed. Moreover, as these variations were performed at a nearly constant HES (about 89%), CO_2 emissions remained largely unchanged.

4. Dual fuel combustion model

As abovementioned, the aim of this paper is the development of a predictive combustion model for dual-fuel operations. More in detail, starting from the model developed by Millo et al. [17] for natural gas-diesel dual-fuel combustion, it has been modified to take into account the hydrogen characteristics.

This model accounts for two combustion modes: diesel spray combustion, which considers not only the combustion of the diesel jet but also the liquid fuel injection, its penetration and evaporation, and then the entrainment of the air-H_2 mixture into the spray. Then, a single spherical flame to model turbulent flame propagation, based on entrainment and burn-up model [24] is employed in the combustion model. A dedicated function is adopted to model the transition between the two modes, spray and turbulent flame combustion. More specifically, this function allows the gradual transition from a truncated cone surface of the spray combustion to a sphere, referred to the flame turbulent combustion.

During the engine cycle simulation, the cylinder region is divided into three thermodynamic zones, each with its own thermodynamic conditions. In detail, the main unburned zone contains the hydrogen-air mixture and the residues from the previous cycle. During the diesel injection, a new zone, known as the spray zone, is created. The diesel is introduced to this zone in accordance with the injection rate, and after

the ignition delay, combustion in the spray is triggered. The onset of spray combustion introduces a new thermodynamic zone, defined as the burned zone. These three zones are capable of exchanging both mass and energy with each other, and the thermodynamic state of each zone is updated at each time step. Therefore, as the combustion process continues, mass and energy are transferred from the main unburned zone and the spray zone to the burned zone, and the rate at which these processes occur is determined by the combustion models employed. After the ignition delay, the modification of which will be analyzed in the following section, the diesel spray combustion is divided into two different contributions: premixed and diffusive combustion.

The modelling of each combustion phase is described in the following subsections.

4.1. Section 4.1 - Penetration, evaporation and entrainment of diesel spray

In the dual-fuel combustion model, the evolution of the diesel spray is described in terms of parcel velocity and penetration. These quantities are evaluated using the model proposed by Jung and Assanis [25]. As discussed in Section 3.1, several studies [22,23] have attributed the enhancement of entrainment to the formation of an entrainment wave following the end of injection. This phenomenon is characterized by two distinct phases: an initial acoustic wave propagating downstream of the diesel jet, followed by a momentum wave traveling at a lower local flow velocity. Both phases contribute to a significant increase in entrainment. To account for this effect, the correlation developed by Zhou et al. [26] was adopted. In this approach, the temporal evolution of spray penetration is modified from a $\sim t^{0.5}$ dependence to $\sim t^{0.25}$ during the deceleration of the spray after the end of injection. The correlations for spray penetration and velocity are reported in Equations (1) and (2), respectively.

$$S=\begin{cases} u_{inj}t\left[1-\frac{1}{16}\left(\frac{t}{t_b}\right)^7\right] & \frac{t}{t_b}\le 1 \\ u_{inj}t_b\frac{15}{16}\left(\frac{t}{t_b}\right)^{0.5} & t_b\le t\le 2t_i \\ u_{inj}\sqrt{2t_b}\,\frac{15}{16}t_i^{0.25}(t-t_i)^{0.25} & t\ge 2t_i \end{cases} \tag{1}$$

$$u=\begin{cases} u_{inj}\left[1-\frac{1}{2}\left(\frac{t}{t_b}\right)^7\right] & \frac{t}{t_b}\le 1 \\ u_{inj}\frac{15}{32}\left(\frac{t}{t_b}\right)^{-0.5} & t_b\le t\le 2t_i \\ u_{inj}\sqrt{\frac{t_b}{2}}\left(\frac{15}{16}\right)t_i^{0.25}(t-t_i)^{-0.75} & t\ge 2t_i \end{cases} \tag{2}$$

Where S is the penetration distance of the parcel, u is the instantaneous parcel velocity, t is the time elapsed since the creation of the parcel, u_{inj} is the velocity of the spray at the injector nozzle, estimated using the mass flow rate profile given as an input to the model, the fuel density and injector nozzle geometry, t_i is the time elapsed between the creation of the parcel and the related end of the injection pulse the parcel belongs to, and t_b is the break-up time, defined as the duration over which the jet behaves as a continuous liquid column before atomization. The breakup time is evaluated according to:

$$t_b=4.351\sqrt{\frac{2\rho_l}{\rho_g}}\,\frac{d_n}{C_d u_{inj}} \tag{3}$$

where ρ_l is the density of the injected liquid, ρ_g is the density of the surrounding gas, d_n is the nozzle hole diameter, and C_d is the discharge coefficient of the injector nozzle.

The entrainment of the hydrogen-air mixture into the diesel spray is computed considering the conservation of the initial momentum of the injected parcel. The entrainment rate is then given by Equation (4)

$$\frac{dm_{ent}}{dt}=-C_{ent}\frac{m_{inj}u_{inj}}{u^2}\frac{du}{dt} \tag{4}$$

where m_{ent} is the mass entrained in the diesel spray, m_{inj} is the injection mass and C_{ent} is the entrainment multiplier. This latter can be utilized to modulate the entrainment of the mixture into the diesel spray on the specific test case under investigation.

The evaporation of the diesel parcel is evaluated based on the work by Morel et al. [27].

4.2. Ignition delay model

The presence of hydrogen affects the ignition delay of the diesel fuel, as discussed in Section 3.1. To account for this effect, 0D detailed chemistry simulations were conducted by means of the CONVERGE CFD software to compute the air-diesel-hydrogen mixture ignition in different thermodynamic conditions and mixture compositions. The Lawrence Livermore National Laboratory (LLNL) reaction mechanism [28] was adopted and the n-dodecane($n-C_{12}H_{26}$) was selected as a surrogate for diesel fuel. A dedicated test matrix was considered with the objective of accurately capturing a wide range of thermodynamic conditions and mixture composition, as shown in Table 4.

The diesel ignition delay predicted by the 0D simulations confirmed the findings reported by Gong et al. [20]. Specifically, at temperatures below 1050 K, the addition of hydrogen led to an increase in ignition delay, indicating an inhibiting effect on diesel ignition. Conversely, at temperatures above 1280 K, hydrogen exhibited an accelerating effect, resulting in a reduced ignition delay.

Several ignition delay correlations have been selected from the available literature. These include the work of Hiroyasu [29], Schmidt [30], Assanis [31], and the correlation available in GT-SUITE [32]. These have been properly tuned to be aligned with the outcomes of detailed chemistry calculations. In particular, only data corresponding to ignition delay times shorter than 0.01 s were considered, as higher values were not representative of engine-relevant conditions. However, as illustrated in Fig. 5, none of them were able to accurately reproduce the outcomes of the 0D computations, since they were not developed to take into account the impact of a secondary fuel on the spray diesel ignition (either acceleration or inhibition).

Therefore, to achieve a more accurate prediction, a different approach has been used in this study. The standard dual-fuel combustion model has been modified with the implementation of a dedicated ignition delay model, which accounts for the impact of the hydrogen on the diesel ignition delay. The detailed chemistry calculation outcomes were utilized to train a multi-layer percept (MLP) neural network. This type of network consists of multiple hidden layers, with each layer comprising a multitude of neurons. Each neuron processes the outcomes from the previous layer using a weighted linear summation, followed by a transfer function that introduces non-linearity into the network [33]. The dataset obtained from the 0D-CFD simulations was randomly divided into training (60%), validation (20%), and test (20%) subsets. The ANN was trained using the machine learning tool available in GT-SUITE. The adopted network consists of four hidden layers with 10, 10, 15, and 10 neurons, respectively. To mitigate overfitting, a

Tables 4
0D simulation test matrix.

Parameter	Minimum value	Maximum value	Interval
Pressure	60 bar	100 bar	5 bar
Temperature	500 K	1600 K	25 K
Equivalence Ratio	0.4	5	0.2
H_2 mass fraction x_{H_2}	0	0.9	0.1
Diesel mass fraction x_D	0.1	1	0.1

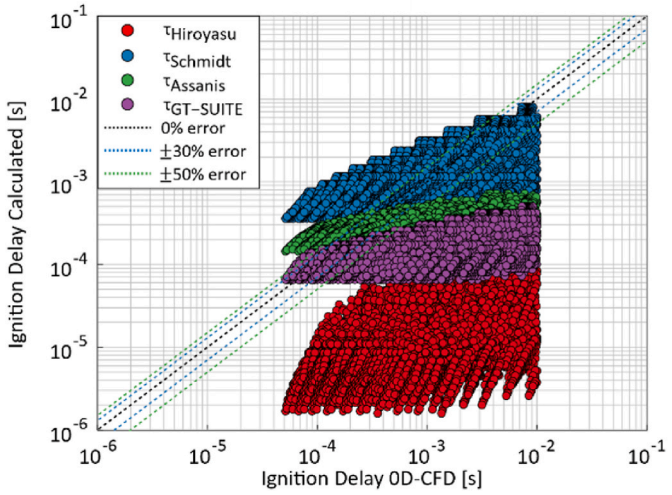


Fig. 5. Comparison of the 0D-CFD calculation outcomes and the ignition delay obtained using different correlations.

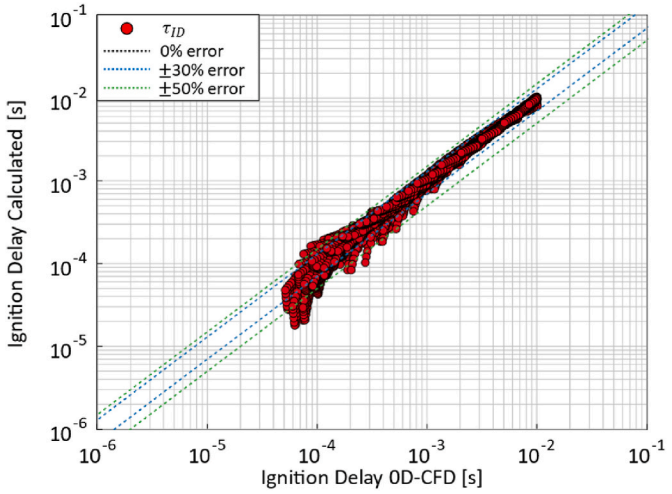


Fig. 6. Comparison of the results of the ANN model and 0D detailed chemistry.

validation set was used during the training process, enabling continuous monitoring of the model performance on unseen data and supporting the tuning of model parameters, as described in the GT-SUITE User's Manual [32]. The trained model was finally evaluated on the test set, confirming its capability to accurately reproduce data not used during training. Fig. 6 shows the results obtained with the ANN model in comparison with the target 0D detailed chemistry calculations. It is evident that the model exhibits a high reliability and, for this reason, it has been adopted in the combustion model as a user subroutine.

4.3. Spray combustion

At the start of combustion, the mixture of diesel and entrained gas in the diesel jet is set aside for the premixed combustion. This process is kinetically-controlled, and the burn rate is computed according to Equation (5).

$$\frac{dm_{pm}}{dt} = C_{pm} m_{pm} k \left(t - t_{ign}\right)^2 f([O_2]) \quad \text{Eq. (5)}$$

where m_{pm} is the premixed mass, k is the turbulent kinetic energy, t is the time, t_{ign} is the time at which the ignition starts, and $f([O_2])$ is a function that accounts for the reduction in combustion intensity caused by decreased oxygen concentration. C_{pm} is a calibration parameter used to tune the premixed burn rate based on experimental data. Subsequently, the residual unmixed fuel keeps mixing with the entrained gas in the jet. The mass of this mixture is known as m_{diff} and burns in a diffusion-limited combustion, given by Equation (6).

$$\frac{dm_{diff}}{dt} = C_{diff} m_{diff} \frac{\sqrt{k}}{\sqrt[3]{V_{cyl}}} f([O_2]) \quad \text{Eq. (6)}$$

Where k is the turbulent kinetic energy, V_{cyl} is the cylinder volume, $f([O_2])$ accounts for the effect of reduced oxygen concentration on combustion intensity. C_{diff} is a calibration parameter used to adjust the diffusion combustion rate.

4.4. Flame propagation model

Moving to the flame propagation, the unburned gas is entrained into the flame front, which starts from the injector location. As the flame front propagates through the combustion chamber, it continuously entrains unburned mixture, which is subsequently consumed behind the flame over a characteristic combustion timescale. At each time step, the evolution of the unburned mass entrained within the flame region, (m_{uf}), is evaluated as the balance between the entrainment rate of fresh mixture and the burn rate occurring behind the flame front (m_{bf}), as shown in Equation (7).

$$\frac{dm_{uf}}{dt} = \rho_u A_e (S_T + S_L) - \frac{dm_{bf}}{dt} \quad \text{Eq. (7)}$$

The entrainment process is assumed to be proportional to the combined contribution of the laminar flame speed, (S_L), the turbulent flame speed, (S_T), the density of the unburned mixture (ρ_u) and the effective flame area (A_e).

The laminar flame speed S_L of the hydrogen combustion is computed by using an artificial neural network (ANN) developed by Gamma Technologies. This ANN was trained using the results of the detailed chemistry simulation, which were obtained considering a wide range of parameters including pressure, temperature, equivalence ratio, and residual gas fraction. The turbulent flame speed is proportional to the turbulence conditions inside the cylinder and is computed as reported in Equation (8).

$$S_T = C_{TFS} u' \left(1 - \frac{1}{1 + \left(\frac{R_f}{L_i}\right)^2} \right) \quad \text{Eq. (8)}$$

Where C_{TFS} is a calibration parameter, u' is the turbulent intensity, and R_f is the flame radius.

4.5. Combustion models coupling

Within the cylinder, two combustion modes coexist simultaneously, making the interaction between them a key aspect of the modelling strategy. For this reason, the proposed framework includes a twofold coupling between spray combustion and turbulent flame propagation.

The first coupling mechanism concerns the evolution of the flame area. At the beginning of combustion, the flame area is assumed to coincide with the external surface of the diesel sprays, whose geometry is approximated as a truncated cone terminated by a hemispherical tip. As combustion develops, the flame progressively evolves from a spray-dominated structure toward a propagating spherical flame. Following an approach similar to that proposed by Walther et al. [34], the equivalent flame area is therefore evaluated as a weighted transition between the spray surface area and the spherical flame surface area. In this formulation, the weighting factor depends on the ratio between the flame radius and the spray penetration length. Consequently, once the flame radius exceeds the spray penetration, the equivalent flame area

fully coincides with that of the spherical propagating flame.

The second coupling mechanism is related to the interaction between the burn rate occurring inside the diesel jets and the burn rate associated with the propagating flame front. As shown in Equations (9) and (10), for the total combustion inside the spray ($\frac{dm_{bs}}{dt}$)and the burn rate due to flame combustion ($\frac{dm_{bf}}{dt}$), respectively, the two combustion rates are mutually dependent.

$$\frac{dm_{bs}}{dt} = \frac{dm_{pm}}{dt} + \frac{dm_{diff}}{dt} + \frac{m_{us}}{m_u}\cdot\frac{dm_{bf}}{dt} \quad \text{Eq. (9)}$$

$$\frac{dm_{bf}}{dt} = \frac{m_{uf}}{\tau} + \frac{m_{bf}}{m_b}\cdot\frac{dm_{bs}}{dt} \quad \text{Eq. (10)}$$

Indeed, since part of the mass within the spray can be burned by the propagating flame and vice versa, an additional term was added for both burn rate calculations. These terms account for the unburned mass within the spray (m_{us}), the overall unburned mass in the cylinder (m_u), the burned mass behind the flame brush (m_{bf}), and total burned mass in the cylinder (m_b). The time characteristic τ is the time necessary to cover the Taylor length scale λ at laminar flame speed and is computed according to Equation (11).

$$\tau = C_{TLS}\cdot\frac{\lambda}{S_L} \quad \text{Eq. (11)}$$

Where C_{TLS} is used as a tuning parameter, while λ is calculated as the ratio between the integral length scale and the square root of the Reynolds number.

This modelling choice originates from the assumption that both the spray combustion process and the flame front are allowed to entrain mass from the entire available unburned mixture. Such mixture includes not only the fresh charge that has not yet been entrained, but also partially entrained regions associated with both the spray and the flame brush. As a consequence, part of the mass initially entrained by the spray may subsequently be consumed by the propagating flame, while mass initially entrained by the flame front may also interact with and be burned within the spray combustion region. In this way, the model introduces a direct interaction between the two combustion modes rather than treating them as fully independent phenomena.

4.6. Flow model

As discussed, the combustion model requires inputs derived from the flow field in the cylinder. For this reason, a flow model needs to be included to determine the turbulence level within the combustion chamber. The 1D-CFD flow model developed by Fogla et al. [35]and based on the K-k-ε approach was chosen for this study. The model calculates the decay of mean kinetic energy (K) to turbulence and computes the integral length scale by evaluating the turbulence kinetic energy (k) and dissipation rate (ε). It includes 3 calibration constants, that have been calibrated having as a reference the outcomes of a 3D-CFD simulations in terms of turbulence kinetic energy (TKE) and the length scale (LS). Two distinct engine working points (WPs) with different valve lifts and diesel SOI were selected, one for the calibration and the other one for the validation of the model. Table 5 indicates the turbulence model calibration constant and the corresponding calibrated values.

Figs. 7 and 8 show the comparison between the turbulence kinetic energy and length scale at start of diesel injection – respectively - resulting from 3D-CFD and from 1D simulations of the calibration and validation working points. The 1D-CFD flow model demonstrated the capacity to replicate both turbulence parameters of the calibration working point at Diesel SOI. The second engine operating point was employed to validate the 1D-CFD turbulence model, keeping unchanged the parameters calibrated in the previous step. The results confirm the previous findings: the calibrated 1D-CFD flow model demonstrated its high capacity to reproduce the turbulence conditions at start of injection of the diesel fuel.

Table 5
Flow model calibration parameters.

Production term multiplier	0.46
Geometric length scale multiplier	0.44
Intake term multiplier	0.11

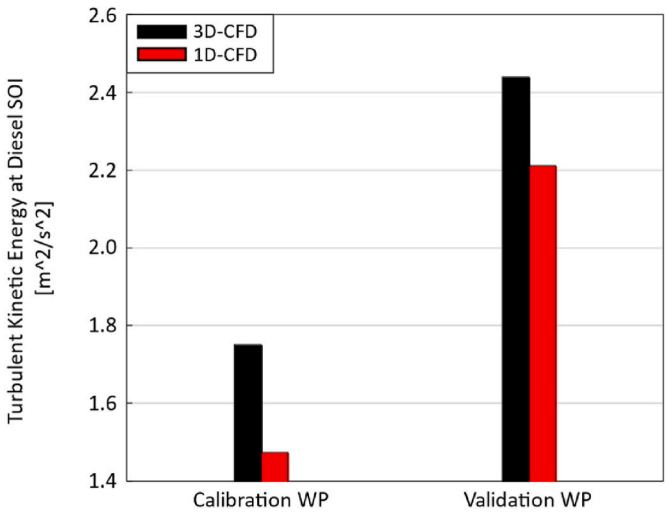


Fig. 7. Turbulent Kinetic Energy (TKE) at Diesel SOI from 3D-CFD and 1D-CFD simulation.

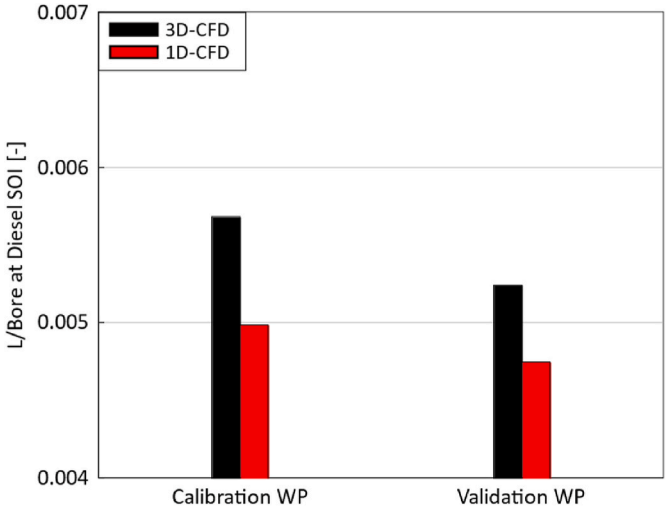


Fig. 8. Length Scale at Diesel SOI from 3D-CFD and 1D-CFD simulation.

4.7. NOx Emissions model

In the present work, the formation of NOx is predicted by employing the well-known Extended Zeldovich model (EZM) [36], which accounts for the main reactions of N_2 oxidation, N oxidation, and OH reduction described in Equations (12)–(14). This approach has been widely adopted for hydrogen–diesel dual-fuel combustion [37], as well as for other dual-fuel applications involving gaseous fuels [17].

$$O + N_2 <=> NO + N \quad (12)$$

$$N + O_2 <=> NO + O \quad (13)$$

$$N + OH <=> NO + H \quad (14)$$

This model relies on the definition of three rate constants, namely k1, k2, and k3, given by Equations (15)–(17), employed to calculate the reaction rate of the EZM reactions.

$$k_1 = 7.60 \cdot 10^{10} \cdot F_1 \cdot e^{-38000\frac{A_1}{T_b}} \tag{15}$$

$$k_2 = 6.40 \cdot 10^{6} \cdot F_2 \cdot T_b \cdot e^{-3150\frac{A_2}{T_b}} \tag{16}$$

$$k_3 = 4.10 \cdot 10^{10} \cdot F_3 \tag{17}$$

Where F_1 indicates the N_2 oxidation rate constant, A_1 represents the N_2 oxidation activation energy constant, T_b is the burned zone temperature, F_2 represents the N oxidation rate constant, A_2 indicates the N oxidation activation energy constant, and F_3 denotes the OH reduction rate constant.

NOx formation is strongly influenced by the temperature history of the burned gases. A significant fraction of the NOx is formed in the burned gases behind the flame front, where the gas mixture continues to be compressed, leading to an increase in temperature and, consequently, in the NOx formation rate. As previously described, the combustion chamber is divided into three thermodynamic zones: unburned, spray, and burned zones. In the present model, NOx formation is evaluated in the burned zone only, using the corresponding temperature evolution. The species concentrations required by the EZM (e.g., O, OH, N) are evaluated assuming chemical equilibrium at the burned-zone thermodynamic conditions.

Therefore, the NOx formation rate is computed based on the burned-zone temperature and the corresponding equilibrium species composition.

5. Results and discussion

The dual fuel combustion model was calibrated against the experimental data by optimizing the six calibration constants summarized in Table 6. These constants were calibrated to minimize the error between the experimental burn rate (averaged considering 100 consecutive engine cycles) and the one predicted by the combustion model. A sensitivity analysis was conducted by varying each calibration parameter independently. The results indicate that each parameter has a distinct effect on the burn rate, influencing both spray combustion and flame propagation, thus supporting the identifiability of the calibrated parameters.

A dataset comprising 30 different engine working conditions (out of a total of 79), randomly selected among the whole dataset, was used as a calibration dataset for the combustion model. The calibration process was carried out in GT-SUITE exploiting the Non-dominated Sorting Genetic Algorithm III (NSGA-III), following the approach of previous studies [17,38]. A single set of tuning parameters was used across the whole set of operating conditions to increase the predictive capabilities of the model. Then, the combustion model was validated on the entire dataset, evaluating the robustness of the model in operating conditions different from the ones used for the calibration.

Fig. 9 presents the outcomes of the combustion model compared with the experimental results. Four different operating conditions variations were evaluated: from top to bottom, hydrogen energy share, hydrogen injection pressure, diesel injection pressure, and diesel SOI at medium engine load. Starting from the sweep of hydrogen energy share (Fig. 9 (a)), the combustion model is able to accurately replicate the variation of the combustion process with the hydrogen fraction. As can be seen from the burn rate curve, reducing the diesel content (from left to right), the intensity of the initial peak, linked to the combustion of the diesel spray, reduces. Conversely, the flame combustion intensity increases due to an increase in the hydrogen-air equivalence ratio. Both phenomena are correctly reproduced by the model. Furthermore, the ignition delay model based on NN trained on the 0D chemistry calculation, confirms its capacity to predict the onset of combustion even considering different share of hydrogen. It is worth to note that some differences arise in the last phase of combustion, regardless of the hydrogen content. Fig. 9(b) illustrates the effect of hydrogen injection pressure. Although the experimental data do not show a significant influence of injection pressure on the burn rate, the model accurately reproduces the combustion behavior. This is expected, as hydrogen is injected via a port fuel injection (PFI) system and, due to its high diffusivity, forms a well-mixed hydrogen–air mixture regardless of the injection pressure. Moving to Fig. 9(c), increasing the diesel injection pressure causes a reduction of the ignition delay. This is mainly due to the improved atomization that reduces the physical delay. Also in this case, the combustion model is capable to predict the impact on the ignition delay. Eventually, the impact of diesel SOI has been analyzed, as shown in Fig. 9(d). As expected, the diesel SOI has a significant impact on the combustion process. Even showing some discrepancies with retarded injection timing, the model is confirmed to be capable to properly predict the combustion process. The deviations observed under retarded injection timing conditions can be attributed to a slightly lower flame propagation speed predicted by the model compared to the experimental behavior, resulting in a reduced peak of the burn rate. This effect is closely related to the start of combustion (SOC), which in these cases occurs approximately 8–10° after TDC. Under such conditions, flame development takes place in a less favorable thermodynamic environment, leading to a reduction in the laminar flame speed as predicted by the model. On the other hand, the spray combustion phase is well reproduced, indicating that the model is still able to capture this combustion phase, even under retarded diesel injection timing conditions.

It is worth noting that some discrepancies arise in the late phase of combustion, regardless of the hydrogen content. These differences are mainly associated with the simplified representation of flame propagation adopted in the model. In particular, during the spray combustion phase, the flame is represented through a truncated-cone surface, while at later stages a transition occurs and the flame is modeled as a single spherical front. This transition does not fully capture the actual evolution of the flame as it propagates from the piston bowl into the squish region, leading to an overestimation of the flame surface area during the final stage of combustion.

As a consequence, the model tends to predict the occurrence of a third peak in the burn rate during the last phase of combustion. This behavior highlights a limitation of the current modeling approach, which will be addressed in future developments through the adoption of a multi-flame framework.

Fig. 10 illustrates the sweep of the hydrogen energy share at high engine load. As demonstrated at medium-load, the combustion model is capable to replicate the combustion behavior as the diesel content is reduced. Additionally, the ignition delay model is able to accurately predict the onset of combustion under higher pressure and temperature conditions at Diesel SOI.

To provide the full picture, the correlation plots in Fig. 11 show the comparison between predictions and experiments for the main combustion parameters for the whole validation dataset. Starting from the left, the crank angle at 5% burned mass (MFB5) plot shows that the combustion model accurately predicted the ignition delay, thus confirming the reliability of the dedicated ignition delay model. Also the crank angle at 50% burned mass (MFB50) is accurately predicted, with a root mean square error (RMSE) of 1.2 CAD on the overall dataset. A

Table 6
Dual-fuel combustion model tuning parameters.

C_{ign}	Ignition delay constant	0.81
C_{ent}	Entrainment rate constant	1.10
C_{pm}	Premixed combustion rate constant	0.87
C_{diff}	Diffusive combustion rate constant	1.49
C_{TFS}	Turbulent flame speed constant	2.30
C_{TLS}	Taylor length scale constant	0.80

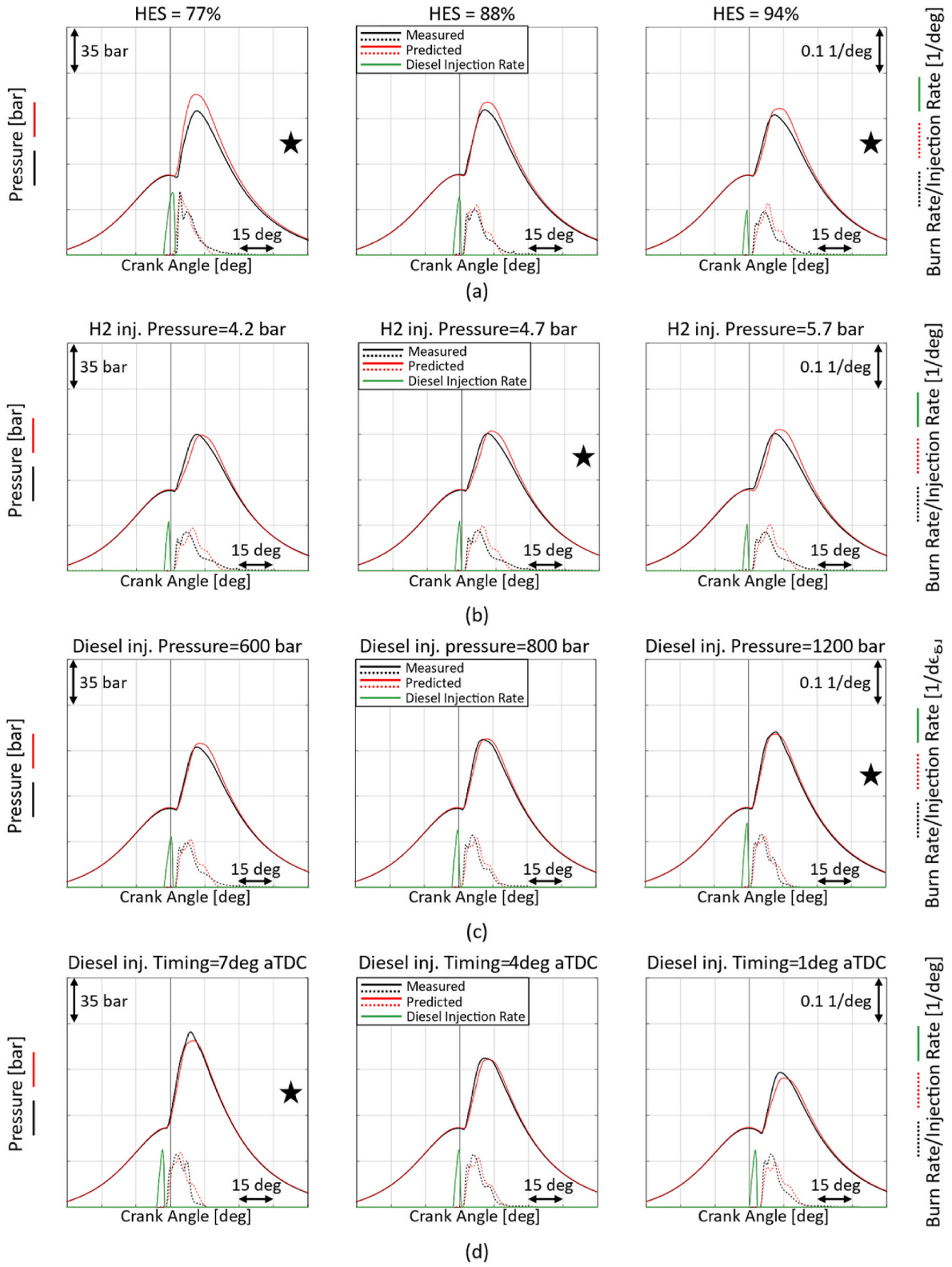


Fig. 9. Evaluation of the difference between predicted (red lines) and measured (black lines) in-cylinder pressure and burn rate (HRR): (a) HES variation with medium-load, (b) Hydrogen injection pressure variation, (c) Diesel injection pressure variation, (d) Diesel SOI variation. The black star indicates an operating condition used for calibrating the combustion model. (For interpretation of the references to colour in this figure legend, the reader is referred to the Web version of this article.)

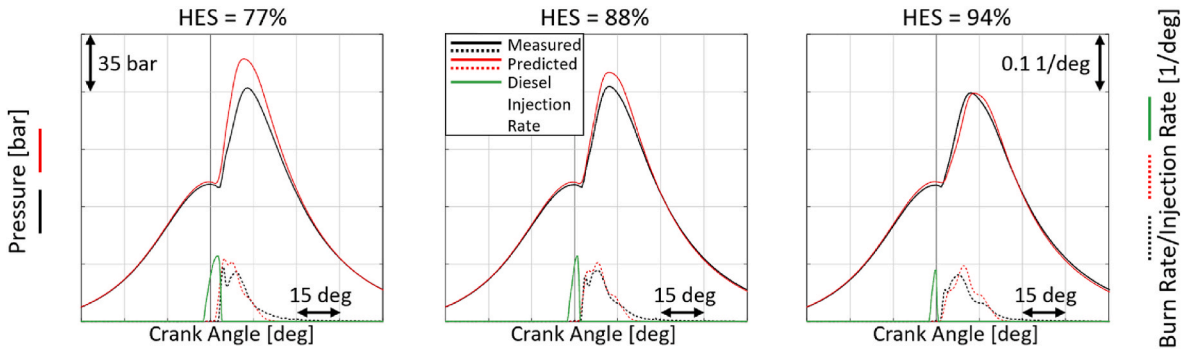


Fig. 10. Comparison of the predicted and measured in-cylinder pressure and burn rate with HES variation under high-load engine conditions.

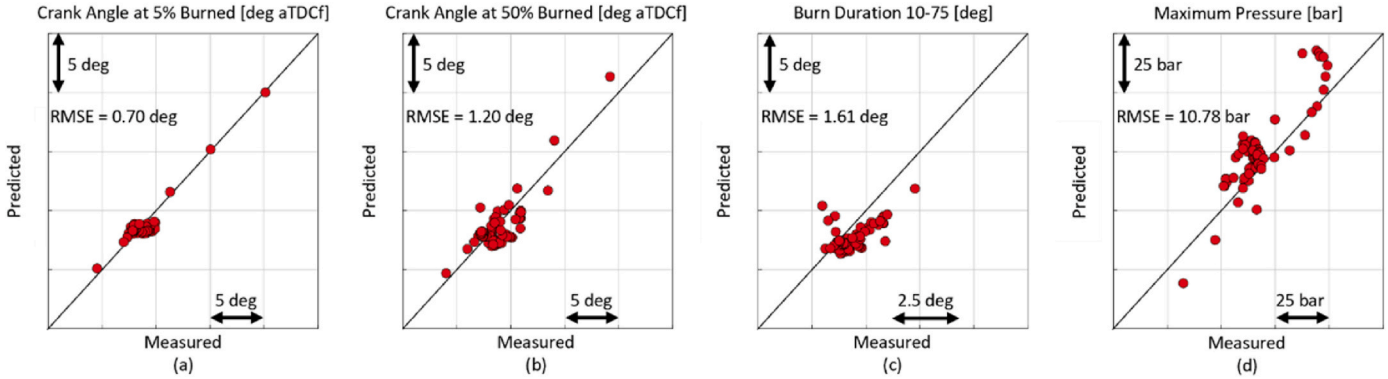


Fig. 11. Correlation plot between predicted and experimental outcomes: from left to right (a) MFB5, (b) MFB50, (c) burn duration 10-75, (d) maximum pressure.

higher discrepancy can be seen in the burn duration plot that is mainly due to the abovementioned error in the last phase of combustion, highlighted in Fig. 11. However, the RMSE is lower than 2 deg, thus highlighting again the robustness of the model. Lastly, the maximum pressure correlation plot indicates that the predicted pressure was marginally higher than the measured value, with most of the points that lie close to the zero error line.

The analysis was extended to two global performance parameters to further assess the robustness of the developed model. Fig. 12 shows the correlation between measured and predicted values of indicated mean effective pressure (IMEP, Fig. 12(a)) and indicated specific fuel consumption (ISFC, Fig. 12(b)). The results show that the model is able to reproduce both quantities with good accuracy over the investigated operating conditions. In particular, IMEP is predicted with a low RMSE (approximately 0.16 bar), while ISFC also shows good agreement between measured and predicted values.

Fig. 13 presents a comparison of the predicted and measured emissions. As shown, the NOx emissions model accurately reproduced the measured emissions, with approximately 70% of the engine operating points exhibiting an error within ±20% and a root mean square error (RMSE) of about 250 ppm over the entire dataset. Fig. 14 compares the predicted and measured emissions for various engine parameter sweeps. Three different operating parameter sweeps were analyzed: hydrogen energy share variation at high-load conditions (Fig. 14(a)), hydrogen injection timing variation (Fig. 14(b)), and diesel injection timing sweep (Fig. 14(c)).

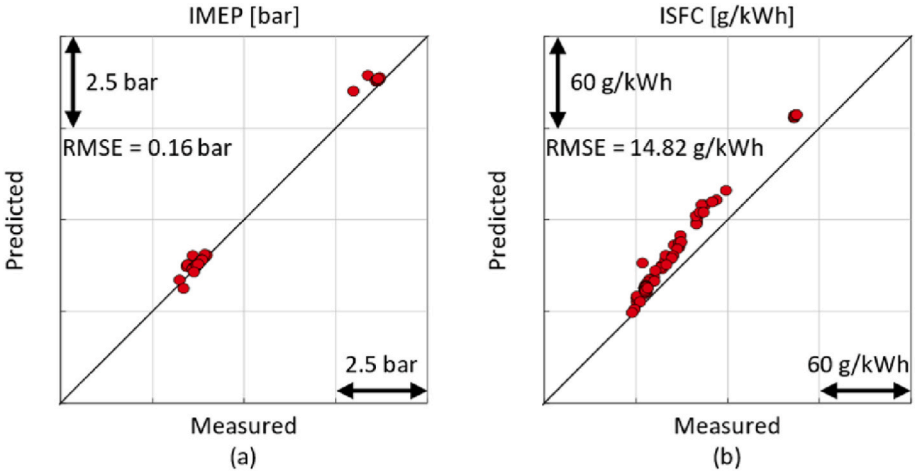


Fig. 12. Correlation plot between predicted and experimental outcomes: (a) IMEP, (b) ISFC.

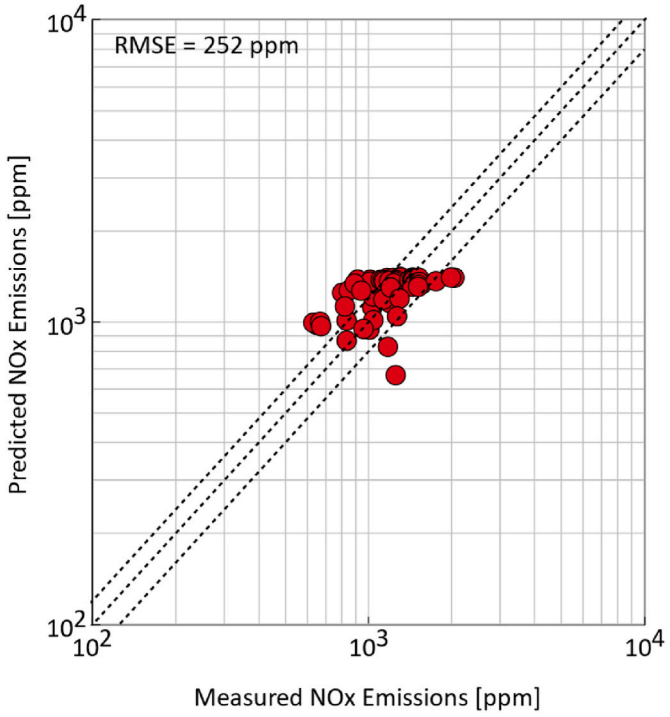


Fig. 13. Correlation plot between measured and predicted NOx emissions.

Starting from the variation in hydrogen energy share at high engine load. As outlined in Section 3.2, an increase in the HES was observed to correspond to higher measured emissions, reaching their maximum at approximately 80%. However, a subsequent increase in the hydrogen energy fraction led to a decline in NOx emissions. The NOx model demonstrated its capacity to predict the emissions trend as the hydrogen content was varied. In this instance, the reduction in ignition delay as the HES increased led to an advancement in the combustion process. Consequently, this resulted in an increase in the in-cylinder pressure and, thus, an increase in the burned mass temperature.

Moving to Fig. 14(b), delaying the hydrogen injection timing does not impact NOx emissions. This behavior indicates that the hydrogen port fuel injection allows for the formation of a well-mixed hydrogen-air mixture, even when the injection is delayed. Consequently, the combustion process was almost the same in all cases. Also in this case, the emissions model is able to simulate the impact of the delayed hydrogen injection timing.

Ultimately, the effect of diesel SOI was evaluated, as illustrated in Fig. 14(c). The NOx emissions exhibit a strong correlation with the diesel SOI. A reduction in NOx emissions is visible by delaying the start of the injection. The emission model demonstrates a qualitative agreement with experimental NOx emissions. Discrepancies were observed when the most advanced and most delayed injection timing were employed. This is due to a slightly lower predicted in-cylinder pressure and temperature with respect to the experimental data.

6. Conclusion

In this study, the conversion of a direct injection compression ignition (DICI) internal combustion engine to operate in hydrogen-diesel dual fuel mode was evaluated. A comprehensive experimental campaign was conducted to investigate the impact of various engine parameters on performance and emissions. The outcomes of this campaign have been employed to develop a suitable combustion model capable of replicating the ignition and combustion processes, as well as the emissions in a dual-fuel engine.

The experimental analysis was conducted to investigate the impact of main engine parameters, including engine load, hydrogen energy share, diesel injection pressure, and timing, on engine performance and NOx emissions. The main outcomes can be summarized as follows.

- The hydrogen energy share exhibited a substantial impact on the ignition delay. The delay evidenced a slight increase until the hydrogen reached approximately 60-70%. Further increases in hydrogen content caused a significant reduction in the delay. The observed behavior can be attributed to the entrainment waves generated at the end of the diesel injection, which enhance the entrainment of the hydrogen-air mixture into the diesel spray. This leads to an increase in the A/F ratio and, consequently, a reduction in ignition delay.
- Furthermore, an increase in nitrogen oxides emissions was observed as the hydrogen energy share increased up to 80%. An further increase in the hydrogen fraction led to a reduction in emissions. This behavior was a consequence of the initial hydrogen addition enhancing the first burn rate peak, leading to higher NOx emissions, whereas higher hydrogen fractions (>80%) reduced NOx due to the reduced amount of diesel.

The well-known dual fuel combustion model, already available in GT-SUITE, was employed to accurately predict the interaction and the transition between the spray combustion of diesel and hydrogen flame combustion. Several modifications have been made to the standard model to enhance its capacity to replicate the effects of varying hydrogen energy shares and diesel and hydrogen injection strategies. To this aim, an ignition delay model was developed by using an artificial neural network trained with the outcomes of the detailed chemistry calculation. Moreover, the penetration spray model was modified to account for the increase of the hydrogen-air mixture entrainment within

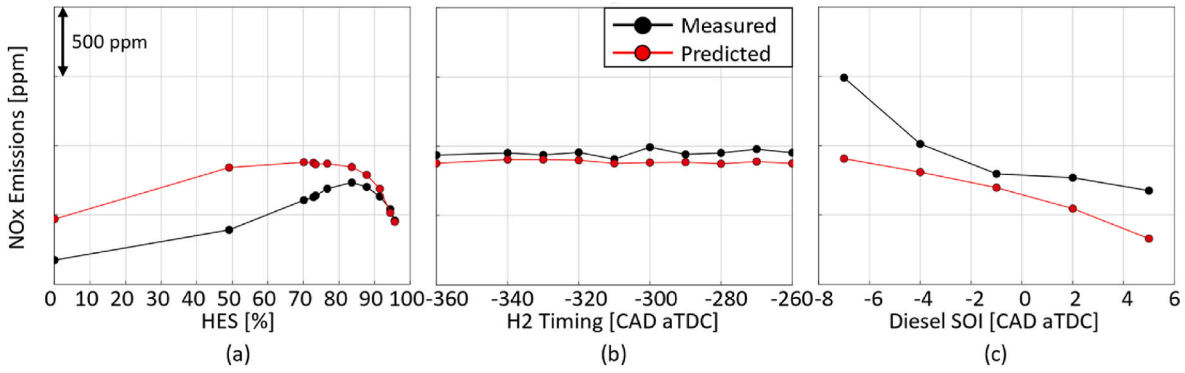


Fig. 14. Comparison between the measured (black dots) and the predicted (red dots) NOx emissions: (a) HES variation with high-load, (b) Hydrogen injection timing variation, (c) Diesel SOI variation. (For interpretation of the references to colour in this figure legend, the reader is referred to the Web version of this article.)

the diesel spray induced by the entrainment wave. Subsequently, the developed ignition delay model and the spray evolution model were integrated into the dual-fuel combustion model. This latter was calibrated and validated against experimental data, thereby demonstrating its capacity to replicate the effects of the variation of the hydrogen energy share on combustion onset and burn rate. Furthermore, the model's capabilities have been evaluated by assessing its ability to predict the combustion process when the pressure and timing of diesel injection are varied.

Additionally, the capabilities of the simulation tool have been enhanced by the implementation of the Extended Zeldovich mechanism, which is employed for the prediction of nitrogen oxides (NOx) emissions. The calibration of this emissions model was carried out using measured NOx emissions as a reference. The developed model accurately replicated the behavior of the NOx emissions as the hydrogen energy share increased. Although the model captures the overall NOx trends across the investigated operating conditions, non-negligible discrepancies remain for some cases. In particular, deviations of about 250 ppm are observed on average, while for a limited number of operating points the error approaches 500 ppm. This highlights a limitation of the current NO(_x) sub-model in terms of absolute prediction accuracy, despite its satisfactory ability to capture the overall emission behavior.

The future development of the combustion model will prioritize enhancing its predictive capabilities. To this end, the model will adopt a multiple-flame approach, aiming to improve the simulation of the diesel spray combustion and the transition from this to the hydrogen flame propagation. This multi-kernel approach is expected to improve the prediction of the late combustion phase.

Moreover, the validation of the developed simulation model is currently limited to medium and high load conditions due to the lack of experimental data at low load, as well as the unavailability of intermediate HES data. Future work will focus on extending the validation to low-load operating conditions and intermediate HES values in order to further assess the model robustness and its capability to accurately reproduce these operating regimes.

CRediT authorship contribution statement

Gerardo Stanzione: Data curation, Formal analysis, Investigation, Methodology, Software, Validation, Visualization, Writing – original draft. **Andrea Piano:** Conceptualization, Investigation, Methodology, Supervision, Visualization, Writing – review & editing. **Federico Millo:** Funding acquisition, Project administration. **Giovanni Vichi:** Conceptualization, Methodology, Project administration, Supervision, Writing – review & editing. **Niccolò Fiorini:** Conceptualization, Methodology, Supervision.

Declaration of competing interest

The authors declare that they have no known competing financial interests or personal relationships that could have appeared to influence the work reported in this paper.

Acknowledgement

This publication is part of the project PNRR-NGEU which has received funding from the MUR – DM 352/2022

References

[1] SLOCAT. Tracking trends in a time of change: the need for radical action towards sustainable transport decarbonisation. Transport and climate change global status report. second ed. 2021. www.tcc-gsr.com.
[2] International Maritime Organization. Nitrogen Oxides (NOx)—Regulation 13. Air Pollut GHG Emiss January 2013.
[3] International Maritime Organization. Sulphur oxides (SOx) and particulate matter (PM)—Regulation 14. Air Pollut GHG Emiss January 2013.
[4] Onorati A, Payri R, Vaglieco B, et al. The role of hydrogen for future internal combustion engines. Int J Engine Res 2022;23(4):529–40. https://doi.org/10.1177/14680874221081947.
[5] Lata DB, Misra A, Medhekar S. Effect of hydrogen and LPG addition on the efficiency and emissions of a dual fuel diesel engine. Int J Hydrogen Energy 2012;37(7):6084–96. https://doi.org/10.1016/j.ijhydene.2012.01.014.
[6] Jukneleviˇcius R, Rimkus A, Pukalskas S, Matijošius J. Research of performance and emission indicators of the compression-ignition engine powered by hydrogen - diesel mixtures. Int J Hydrogen Energy 2019;44(20):10129–38. https://doi.org/10.1016/j.ijhydene.2018.11.185.
[7] Sharma P, Dhar A. Effect of hydrogen supplementation on engine performance and emissions. Int J Hydrogen Energy 2018;43(15):7570–80. https://doi.org/10.1016/j.ijhydene.2018.02.181.
[8] Vadlamudi S, Gugulothu SK, et al. Paradigm analysis of performance and exhaust emissions in CRDI engine powered with hydrogen and Hydrogen/CNG fuels: a green fuel approach under different injection strategies. Int J Hydrogen Energy 2023;48(96):38059–76. https://doi.org/10.1016/j.ijhydene.2022.08.277.
[9] Tashie-Lewis B, Nnabuife S. Hydrogen production, distribution, storage and power conversion in a hydrogen economy - a technology review. Chem Eng J Adv 2021;8:100172. https://doi.org/10.1016/j.ceja.2021.100172.
[10] Karimi M, Wang X, Hamilton J, Negnevitsky M, Lyden S. Status, challenges and opportunities of dual fuel hybrid approaches-a review. Int J Hydrogen Energy 2021;46(70):34924–57. https://doi.org/10.1016/j.ijhydene.2021.08.008.
[11] Liu X, Liu S, Shen L, Bi Y, Duan L. Study on the effects of the hydrogen substitution rate on the performance of a hydrogen–diesel dual-fuel engine under different loads. Energies 2023;16:5971. https://doi.org/10.3390/en16165971.
[12] Gurusamy M, Subramanian B. A comprehensive analysis of a dual fuel engine operating on cottonseed oil methyl ester and hydrogen. Fuel 2025;383:133789. https://doi.org/10.1016/j.fuel.2024.133789.
[13] Chetia B, Debbarma S, Das B. Enhancing engine performance, combustion, and emissions characteristics through CeO2-modified cottonseed biodiesel with hydrogen enrichment: a comprehensive investigation. Int J Hydrogen Energy 2024;89:1149–65. https://doi.org/10.1016/j.ijhydene.2024.09.417.
[14] Parsa S, Verhelst S. Determining pilot ignition delay in dual-fuel medium-speed marine engines using methanol or hydrogen. Energies 2025;18(12):3064. https://doi.org/10.3390/en18123064.
[15] Barro C, Nani C, Hutter R, Boulouchos K. Spray model based phenomenological combustion description and experimental validation for a dual fuel engine. SAE technical paper 2017-24-0098. 2017. https://doi.org/10.4271/2017-24-0098.
[16] Taritas I, Kozarac D, Sjeric M, Sierra Aznar M, et al. Development and validation of a quasi-dimensional dual fuel (Diesel – natural gas) combustion model. SAE Int J Engines 2017;10(2):483–500. https://doi.org/10.4271/2017-01-0517.
[17] Millo F, Accurso F, Piano A, Fogla N, et al. Development and validation of a multi-zone predictive combustion model for large-bore DualFuel engines. SAE Int J Engines 2022;15(5). https://doi.org/10.4271/03-15-05-0038.
[18] Metghalchi M, Keck JC. Burning velocities of mixtures of air with methanol, isooctane, and indolene at high pressure and temperature. Combust Flame 1982;48:191–210. https://doi.org/10.1016/0010-2180(82)90127-4.
[19] Dhole AE, Yarasu RB, Lata DB. Investigations on the combustion duration and ignition delay period of a dual fuel diesel engine with hydrogen and producer gas as secondary fuels. Appl Therm Eng 2016. https://doi.org/10.1016/j.applthermaleng.2016.06.151.
[20] Gong X, Wang X, Zhou H, Ren Z. Laminar flame speed and autoignition characteristics of surrogate jet fuel blended with hydrogen. Proc Combust Inst 2023;39(2):1773–81. https://doi.org/10.1016/j.proci.2022.07.162.
[21] Frerichs J, Eilts P. Development of a physically/chemically based approach for 2-Stage ignition delay calculation in medium speed dual-fuel engines. SAE technical paper. 2019. https://doi.org/10.4271/2019-24-0068.
[22] Musculus M, Kattke K. Entrainment waves in diesel jets. SAE Int J Engines 2009. https://doi.org/10.4271/2009-01-1355.
[23] Musculus M. Entrainment waves in decelerating transient turbulent jets. J Fluid Mech 2009;638:117–40. https://doi.org/10.1017/S0022112009990826.
[24] Morel T, Rackmil CI, Keribar R, Jennings MJ. Model for heat transfer and combustion in spark ignited engines and its comparison with experiments. SAE tech pap. 1988. https://doi.org/10.4271/880198.
[25] Jung D, Assanis DN. Multi-zone di diesel spray combustion model for cycle simulation studies of engine performance and emissions. SAE technical papers, 724; 2001. https://doi.org/10.4271/2001-01-1246.
[26] Zhou X, Li T, Lai Z, Wei Y. Modeling diesel spray tip and tail penetrations after end-of-injection. Fuel 2019;237:442–56. https://doi.org/10.1016/j.fuel.2018.10.029.
[27] Morel T, Wahiduzzaman S. Modeling of diesel combustion and emissions. XXVI FISITA Congress. 1996.
[28] Lapointe S, Zhang K, McNenly MJ. Reduced chemical model for low and high-temperature oxidation of fuel blends relevant to internal combustion engines. Proc Combust Inst 2019;37(1):789–96. https://doi.org/10.1016/j.proci.2018.06.139.
[29] Hiroyasu H, Kadota T, Masataka A. Development and use of spray combustion modeling to predict diesel engine efficiency and pollutant emissions. Jpn Soc Mech Eng - JSME 1983;26(214):569–75. https://doi.org/10.1299/jsme1958.26.569.
[30] Schmidt F. Theoretical and experimental study of ignition lag and engine knock. NTRS - NASA Technical Reports 1939.
[31] Assanis DN, Filipi ZS, Fiveland SB, Syrimis M. A predictive ignition delay correlation under steady-state and transient operation of a direct injection diesel engine. J Eng Gas Turbines Power 2003;125(2):450–7. https://doi.org/10.1115/1.1563238.

[32] Gamma Technologies. GT-Suite User's manual. 2024.
[33] Uhlig S, Alkhasli I, Schubert F, Tschöpe C, Wolff M. A review of synthetic and augmented training data for machine learning in ultrasonic non-destructive evaluation. Ultrasonics 2023;134:107041. https://doi.org/10.1016/j.ultras.2023.107041.
[34] Walther H-P, Schlatter S, Wachtmeister G, Boulouchos K. Combustion models for lean-burn gas engines with pilot injection. MTZ Worldw 2012;73(2):56–63. https://doi.org/10.1365/s38313-012-0144-3.
[35] Fogla N, Bybee M, Mirzaeian M, Millo F, Wahiduzzaman S. Development of a K-k-ε phenomenological model to predict in-cylinder turbulence. SAE Int J Engines 2017;10(2):1–14. https://doi.org/10.4271/2017-01-0542.
[36] Heywood JB. *Internal combustion engine fundamentals*. New York: McGraw-Hill; 1988.
[37] Kumar M, Tsujimura T, Suzuki Y. NOx model development and validation with diesel and hydrogen/diesel dual-fuel system on diesel engine. Energy 2017. https://doi.org/10.1016/j.energy.2017.12.148.
[38] Millo F, Boccardo G, Piano A, Arnone L, et al. Numerical simulation of the combustion process of a high EGR, high injection pressure, heavy duty diesel engine. SAE technical paper. 2017. https://doi.org/10.4271/2017-24-0009.